

TRACING THE STAR FORMATION-DENSITY RELATION TO $Z \sim 2$

RYAN F. QUADRI^{1,2,3}, RIK J. WILLIAMS¹, MARIJN FRANX³, HENDRIK HILDEBRANDT⁴

Submitted to the Astrophysical Journal

ABSTRACT

Recent work has shown that the star formation-density relation — in which galaxies with low star formation rates are preferentially found in dense environments — is still in place at $z \sim 1$, but the situation becomes less clear at higher redshifts. We use mass-selected samples drawn from the UKIDSS Ultra-Deep Survey to show that galaxies with quenched star formation tend to reside in dense environments out to at least $z \sim 1.8$. Over most of this redshift range we are able to demonstrate that this star formation-density relation holds even at fixed stellar mass. The environmental quenching of star formation appears to operate with similar efficiency on all galaxies regardless of stellar mass. Nevertheless, the environment plays a greater role in the build-up of the red sequence at lower masses, whereas other quenching processes dominate at higher masses. In addition to a statistical analysis of environmental densities, we investigate a cluster at $z = 1.6$, and show that the central region has an elevated fraction of quiescent objects relative to the field. Although the uncertainties are large, the environmental quenching efficiency in this cluster is consistent with that of galaxy groups and clusters at $z \sim 0$. In this work we rely on photometric redshifts, and describe some of the pitfalls that large redshift errors can present.

Subject headings: galaxies: evolution – galaxies: high-redshift – galaxies: clusters: general – cosmology: large-scale structure of the universe

1. INTRODUCTION

One of the most striking features of the galaxy population at low redshift is the correlation between galaxy properties — notably, mass, morphology, and star formation rate — and the local environmental density (e.g. Dressler 1980; Balogh et al. 1998; Gómez et al. 2003; Kauffmann et al. 2004; Weinmann et al. 2006). Although significant work has gone into understanding these relationships from both an observational and a theoretical point of view, we still have a limited understanding of the role of environment in shaping galaxy properties and of the specific physical processes through which the environment operates. In this context, it may be expected that extending the observations to higher redshift will provide new insight.

In this paper we investigate the evolution of the star formation-density relation, in which galaxies in dense regions tend to have lower star formation (SF) rates than galaxies in the field. A number of studies in recent years have used statistical measures of environmental densities to investigate this very issue, and have mostly concluded that the SF-density relation disappears, or even “reverses,” at $z \sim 1$ (e.g. Cucciati et al. 2006; Cooper et al. 2007; Elbaz et al. 2007; Ideue et al. 2009; Salimbeni et al. 2009; Scodreggio et al. 2009; Tran et al. 2010; Grützbauch et al. 2011a). But several of these studies do find robust environmental effects out to $z \sim 0.8$ – 1 (see also Scoville et al. 2007; Patel et al. 2009b, 2011; Cooper et al. 2010), which implies a fairly sharp transition at $z \sim 1$.

However there are several reasons to doubt the existence of such a strong transition. Given the apparently smooth growth of the red sequence over cosmic time (Brammer et al. 2009; Williams et al. 2009; Ilbert et al. 2010; Kajisawa et al. 2011), it would be odd if this growth occurred preferentially in overdense regions at $z < 1$ but avoided them at $z > 1$. Instead, there are several examples of clusters at $z \sim 1.5$ that already have prominent populations of passive galaxies in place (e.g. McCarthy et al. 2007; Kurk et al. 2009; Wilson et al. 2009; Strazzullo et al. 2010). Studies of galaxy clustering have also found that red galaxies tend to be more clustered than blue galaxies at $z \gtrsim 1.5$ (e.g. Grazian et al. 2006; Quadri et al. 2007, 2008; Hartley et al. 2010), which also suggests that they reside in denser environments. Moreover, if nothing else, it is natural to expect that more massive galaxies at $z > 1$ should tend to lie in denser environments, and given that more massive galaxies are also more likely to have their star formation quenched (“downsizing”), this would suggest that the SF-density relation should extend to $z > 1$.

Several of the studies that have performed direct estimates of environmental densities have used large samples of galaxies with spectroscopic redshifts, however obtaining spectroscopic redshifts for large and unbiased samples at $z > 1$ is very difficult. Quiescent galaxies, which are very faint in the observer’s optical, are especially hard to observe, and it is these galaxies that are of particular interest when studying the SF-density relation. A second, although perhaps less significant, difficulty for spectroscopic studies is obtaining sufficiently dense spectroscopic sampling of galaxies in overdense regions.

Other studies have estimated environmental densities using photometric redshifts. This has the obvious advantage of providing less biased samples, and is also not subject to the geometrical constraints imposed by multi-

quadri@obs.carnegiescience.edu

¹ Carnegie Observatories, Pasadena, CA 91101

² Hubble Fellow

³ Leiden Observatory, Leiden University, NL-2300 RA, Leiden, Netherlands

⁴ University of British Columbia, Vancouver, B.C. V6T 2C2, Canada

object spectrographs. However these studies have the tremendous disadvantage of large redshift errors, making it virtually impossible to confirm the membership of any one individual galaxy in an observed overdensity, or to know whether an apparent overdensity is a single structure or simply arises in projection. But the hope is that by using a large enough sample it will be possible to tell whether galaxies of one type tend to have, on average, a greater or fewer number of near neighbors with similar photometric redshifts than galaxies of another type.

In this paper we wish to study the evolution of the SF-density relation out to $z \sim 2$ using mass-selected samples, as this is expected to give a more representative view of environmental effects than flux- or luminosity-selected samples (e.g. Patel et al. 2009b). Because many of the most massive galaxies, and in particular those with quenched star formation, are very faint in the observer’s optical, it is not feasible with current telescopes to obtain large spectroscopic samples. This forces us to rely on photometric redshifts.

We separate the quiescent from the star forming galaxies using the observed bimodality in a color-color diagram, which is model-independent and has a significant advantage over the traditional color-magnitude diagram in that it removes contamination of the “red sequence” by dusty star-forming galaxies. The SF-density relation is then quantified using the fraction of quiescent galaxies in different environments. The dataset is described in §2, and in §3 we discuss how we estimate the environmental densities, taking care to note the ways in which the use of photometric redshifts can actually introduce artificial environmental trends. The results are presented in §4, and in §5 we consider the particular case of a cluster at $z=1.62$. Conclusions are given in §6. In the Appendix we discuss some additional details of the relationships between stellar mass, star formation, and environmental density, and we demonstrate the relative importance of environmental processes in the build-up of the red sequence.

2. DATA AND OBJECT SELECTION

2.1. Imaging data

Here we use public data in the field covered by the UKIDSS Ultra-Deep Survey (UDS; O. Almaini 2011, in preparation).⁵ This field has extensive imaging in the optical, near-infrared (NIR), and infrared (IR). The NIR data comes from the UKIDSS survey, which is described by Lawrence et al. (2007). The photometric system and calibration are described by Hewett et al. (2006) and Hodgkin et al. (2009), respectively. Optical $BVRi'z'$ imaging in this field comes from the Subaru/*XMM* Deep Survey (Furusawa et al. 2009), with additional u^* -band taken with MEGACAM on the Canada-France Hawaii Telescope (P.I. O. Almaini). We use *Spitzer*/IRAC and MIPS photometry from the *Spitzer*-UDS Survey (SpUDS; P.I. J. Dunlop). The IR fluxes were measured using the PSF-convolution procedure of Labbé et al. (2006). The area of the field with full multiwavelength imaging is $\sim 0.65\text{deg}^2$.

We update our previous photometric K -selected catalog of the UDS (described in Williams et al. 2009) us-

ing Data Release 8 of the UKIDSS NIR imaging, which reaches 5σ point-source depths of $J = 24.9$, $H = 24.1$, and $K = 24.5$ (AB magnitudes). We also update the optical photometry using SXDS Data Release 1, and use the SpUDS IR data rather than the shallower data from the *Spitzer* Wide-Area Infrared Extragalactic Survey (SWIRE; Lonsdale et al. 2003). This updated catalog will be described in detail by Williams et al. (2011; in preparation).

2.2. Photometric redshifts

We calculate photometric redshifts with EAZY (Brammer, van Dokkum, & Coppi 2008). We make use of a slightly updated template set (G. Brammer, private communication), and use an iterative zeropoint-tuning procedure which is effective at removing systematic errors in the photometric redshifts. A comparison to a sample of ~ 1500 spectroscopic redshifts drawn from a variety of sources (Simpson et al. 2010, in preparation; Akiyama et al. 2011, in preparation; Smail et al. 2008) suggests a typical uncertainty in $\Delta z/(1+z)$ of 0.018 over $0 < z < 1$, and of 0.022 over $1 < z < 1.5$. An additional comparison to the spectroscopic redshifts of objects in the $z=1.6$ cluster in the UDS (Papovich et al. 2010; Tanaka et al. 2010) gives an uncertainty of ~ 0.03 .

While this analysis suggests that the photometric redshift quality is very good, the spectroscopic redshifts that we have compared to are not representative of the galaxies studied in this paper, so exact values quoted above may not be particularly relevant. And, as discussed in §3, overestimating the quality of the photometric redshifts can introduce spurious signals in environmental studies. We therefore use the procedure of Quadri & Williams (2010) to estimate the true redshift errors: briefly, close pairs of objects on the sky have a significant probability of lying at the same redshift, so the photometric redshift differences in close pairs can be used to estimate the distribution of photometric redshift errors. A statistical correction for close pairs that are due to chance projections is performed by randomizing the galaxy positions and repeating the procedure.

The estimated 1σ photometric redshift errors for the mass-selected samples used in this work are shown in Figure 1. This figure also shows that quiescent galaxies typically have better photometric redshifts than star-forming galaxies, which has implications for our density measurements (§3).

2.3. Object selection: stellar masses and the classification of quiescent galaxies

Stellar masses were determined by fitting Bruzual & Charlot (2003) stellar population synthesis models to the observed optical/NIR/IR photometry using FAST (Kriek et al. 2009)⁶. The models were generated using a Chabrier IMF, solar metallicity, and a range of exponentially-declining star formation histories.

In this paper we limit the sample at $K_{AB} < 24.0$, where an inspection of the galaxy number counts shows that our catalog is essentially 100% complete. This limit corresponds to a K -band signal-to-noise ratio of ~ 8 in

⁶ We note that using the Maraston (2005) models reduces the typical stellar masses by ~ 0.15 dex, with relatively small redshift and mass dependence.

⁵ www.nottingham.ac.uk/astronomy/UDS/

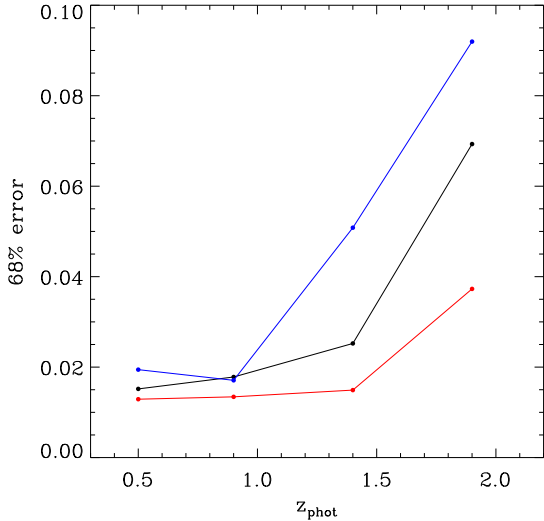


FIG. 1.— The 68% photometric redshift errors in $\Delta z/(1+z)$ for the mass-selected samples used in this work. The errors are estimated by inspecting the difference in photometric redshifts of close pairs of galaxies. The black curve is for the full mass-limited sample, and the red and blue curves are for quiescent and star-forming subsamples, respectively.

the 1.8'' aperture that is used to measure galaxy colors. We estimate the mass completeness limit that corresponds to this flux limit as a function of redshift using a method similar to that of Marchesini et al. (2009): we select galaxies with $23.5 < K < 24.0$, scale their fluxes and masses down to our adopted flux limit of $K = 24.0$, and define the mass completeness limit as the upper end of locus of points in a plot of mass versus redshift.⁷

In this work we select quiescent galaxies using the observed bimodality in a rest-frame $U - V$ versus $V - J$ color-color diagram. This has a significant advantage over the standard color-magnitude diagram that is used to isolate the red sequence in that it successfully separates out dusty star-forming galaxies from those that have suppressed star formation (Williams et al. 2009). And since it is based on the observed bimodality, rather than actual estimates of star formation rates (from e.g. stellar population modeling), it is model-independent. For more discussion, including examples of $U - V$ versus $V - J$ color-color diagrams, we refer the reader to Williams et al. (2009) and Whitaker et al. (2010).

For brevity we refer to the galaxies selected in such a diagram as “quiescent,” although it is possible that they actually have a non-negligible amount of star formation. Currently the most stringent upper limit for such “quiescent” galaxies at $z \sim 2$ comes from the ultra-deep NIR spectroscopy of Kriek et al. (2009), who quote a star formation rate of $< 4M_{\odot}/\text{yr}$ (corresponding to a specific

⁷ This procedure will fail if galaxies at $K > 24$ have significantly higher mass-to-light ratios than galaxies at $K < 24$, as such galaxies would lie above the locus of points if their fluxes (and masses) were scaled up to $K = 24$. However this is not expected to be the case, as, generally speaking, fainter and lower mass galaxies tend to have lower M/L over a wide range in redshift. We have tested our procedure by calculating the mass limit corresponding to $K = 23$ by selecting galaxies at $22.5 < K < 23$ and at $23 < K < 23.5$, scaling the fluxes and masses to $K = 23$, and verifying that these two samples give virtually identical mass completeness limits.

star formation rate of $< 2 \times 10^{-11} \text{yr}^{-1}$), although this is only for a single object. While a galaxy with this much activity would certainly be considered to be star-forming at $z \sim 0$, typical massive star-forming galaxies at these redshifts have at least an order magnitude more star formation.

3. DENSITY ESTIMATION, AND THE USE OF PHOTOMETRIC REDSHIFTS

Two of the simplest, and traditionally the most widely-used, estimators of the local projected density are the distance to the n th nearest neighbor, with n typically varying from 3–10, and the counts within a cylinder, where the radius typically varies from 0.5–8 Mpc. In this work we use the distance to the n th nearest neighbor, as the adaptive nature of this estimator gives somewhat more dynamic range in extreme environments (e.g. Kovač et al. 2010). Although we present results for mass-selected samples, we do not apply a mass limit to the “neighbors” that are used when estimating the local densities. This gives a much higher number of objects on the sky to estimate the densities with and also allows us to measure accurate densities over smaller angular scales, thereby limiting the number of objects that we discard due to edge effects.

In practice we use the distance to the 8th nearest neighbor, which corresponds to roughly ~ 0.5 comoving Mpc over the considered redshift range, but we note that varying n between 5 and 10 yields very similar results. We also obtain similar results if counting only mass-limited objects as “neighbors,” although in this case the length scales that are probed are larger and we have to reduce n to 3–5 in order to limit contamination from objects that are not physically associated with each other. Finally, qualitatively similar results are also obtained by measuring densities within a cylinder with radius 1 comoving Mpc. The good (qualitative) agreement between all of these estimators supports the robustness of our conclusions.

Because the photometric redshifts uncertainties are large when compared to the length scales of structures in the universe and when compared to the true virial motions of objects in groups and clusters, density estimates around individual objects are highly uncertain. Therefore if even a weak trend is apparent in the data, in actuality it must be strong indeed. In the following sections we show correlations between (projected) local density and galaxy properties, which suggests that density estimates using broadband photometric redshifts are still useful and that interesting lessons can still be learned. If these estimates were essentially random numbers then we would not see correlations.

However, photometric redshift errors can actually introduce artificial trends of galaxy properties with density. This is due to the fact that quiescent galaxies tend to have more accurate photometric redshifts than star-forming galaxies (§2.2; see also Quadri & Williams 2010). For example, consider the case of a galaxy overdensity that has the same quiescent fraction as the field, so that no SF-density relation exists. Photometric redshift errors may scatter some fraction of the star-forming galaxies in this overdensity to much higher or lower redshifts, in which case an observer may not consider them to be members of the overdensity at all. Thus the ob-

server would infer that the overdensity is populated primarily by quiescent galaxies, and will mistakenly conclude that an SF-density relation does exist.

The key issue in this example is what difference in photometric redshifts can be tolerated before galaxies will no longer be considered neighbors. If a sufficiently large redshift “linking length” is used, then the star-forming galaxies in the above example would still be considered as possible members of the overdensity, and the hypothetical observer will not be misled. On the other hand, it is desirable not to use too large of a linking length in order to limit contamination from sources that are not physically associated with each other.

An appropriate value for the linking length would be a few times larger than the typical photometric redshift uncertainties for the star-forming galaxies. This makes it important to have an understanding of how the redshift errors depend on galaxy type and on redshift. As described in §2.2 we use the method of Quadri & Williams (2010) to estimate the uncertainties. In practice we use a linking length 3σ . Varying this between 2σ and 4σ yields very similar results; setting a linking length below $\sim 2\sigma$ makes for a stronger SF-density relation, but this additional signal may be partially spurious as per the discussion above. Additionally, we have tested our procedure by adding noise to the redshifts of the quiescent galaxies in order to match the uncertainties for the star-forming galaxies, and our basic conclusions remain unchanged.

A related issue concerns galaxies that fall outside of our redshift bins. When estimating densities for objects near the edge of our redshift bins, we must be sure to also count neighbors if they fall outside of the redshift bin of interest but still within a linking length of the bin. We have found that neglecting this step can introduce a strong artificial signal.

Another way in which artificial correlations of quiescent fraction with density can arise is through the necessity of using galaxy samples that span a range in redshift. Since the quiescent fraction increases with decreasing redshift, and since there is also a slight trend of increasing density with decreasing redshift within our redshift windows, this can introduce an artificial trend of increasing quiescent fraction with increasing density. In practice this does have a minor but noticeable effect on our results, so we subtract out the mean trend of density with redshift within each of our redshift bins.

4. THE STAR FORMATION-DENSITY RELATION

4.1. *Dependence of Quiescent Fraction on Density and Redshift*

We begin by showing the relationship between quiescent fraction and projected density in Figure 2. We apply a mass limit of $\log(M/M_\odot) > 10.2$ in all three redshift bins; this corresponds to our completeness limit at $z = 2$. Two galaxies are considered “neighbors” if they have a photometric redshift separation that is $3 \times \sqrt{2}$ times the estimated redshift uncertainty, where the factor of $\sqrt{2}$ accounts for the fact that both galaxies are subject to redshift errors. The quiescent fractions in this figure are calculated using a running mean, where the width of the box is 0.3 dex in $\log(1 + \delta)$, and the shaded region illustrates the 1σ uncertainties based on Poisson statistics

for the number of quiescent galaxies in a bin.

In agreement with many previous studies, we find a strong star formation-density relation out to $z \sim 1$, but we also find that this trend continues to higher redshifts. In each redshift bin we use a Kolmogorov-Smirnov (K-S) test to calculate the probability that the distribution of densities for the quiescent and star-forming populations are drawn from the same parent distribution. This probability is $\ll 1\%$ in the two lower-redshift bins, but increases to 5% at $1.5 < z_{phot} < 2$, suggesting that the presence of a SF-density relation is still significant at the $\sim 2\sigma$ level at these redshifts. We also show the typical local density and quiescent fraction for candidate members of a $z = 1.6$ cluster in the rightmost panel in this figure; this cluster will be discussed in §5. The cluster candidates have high densities as estimated using the 8th nearest-neighbor statistic, and also have a significantly elevated quiescent fraction relative to the field. Thus this cluster reinforces our conclusion that the SF-density relation is in place at $z > 1.5$.

Recently two studies have presented a similar analysis as shown here using earlier data releases of the UDS. Tran et al. (2010) find that the SF-density relation has reversed by $z \sim 1.6$, whereas Chuter et al. (2011) find a normal relation over $1.25 < z < 1.75$. Our analysis is in agreement with the latter study, but the reasons for the disagreement with Tran et al. (2010) are unclear.

4.2. *The role of stellar mass in the SF-density relation*

A physical interpretation of the relationship between quiescent fraction and density that was shown in the previous subsection is complicated by the effects of stellar mass. Since the fraction of quiescent objects increases with mass, and given the expectation that more massive galaxies will tend to be found in denser regions, it is likely that the observed SF-density relation is at least partially due to a combination of the underlying SF-mass and mass-density relations. While in the local universe it is well-known that environmental trends persist even at fixed stellar mass (e.g. Hogg et al. 2003; Baldry et al. 2006; van den Bosch et al. 2008; Peng et al. 2010), the situation is less clear at higher redshifts: Patel et al. (2009b) and Cooper et al. (2010) find that the same is true at $z \sim 0.9$, but other studies (Scodreggio et al. 2009; Iovino et al. 2010; Grützbauch et al. 2011b) have suggested that any environmental trends at these higher redshifts are solely due to trends with stellar mass. If this is true, it may be that these trends should not be considered to be “environmental” at all.

The relationship between stellar mass and the SF-density relation is demonstrated in Figure 3, where we show the mean densities of star-forming and quiescent galaxies in narrow 0.2 dex bins of stellar mass. Over such narrow bins, the difference in mean stellar mass between the star-forming and quiescent galaxies is never more than 0.025 dex (and is usually much less), which is not enough to account for a significant change in density. The error bars are the standard deviation of the mean.

There are several noteworthy features of this figure. One is that, as mentioned above, out to at least $z \sim 1.25$, quiescent galaxies tend to be found in denser environments than star-forming galaxies even at fixed mass. For the star-forming galaxies, there is a clear and apparently monotonic increase in mean density with stel-

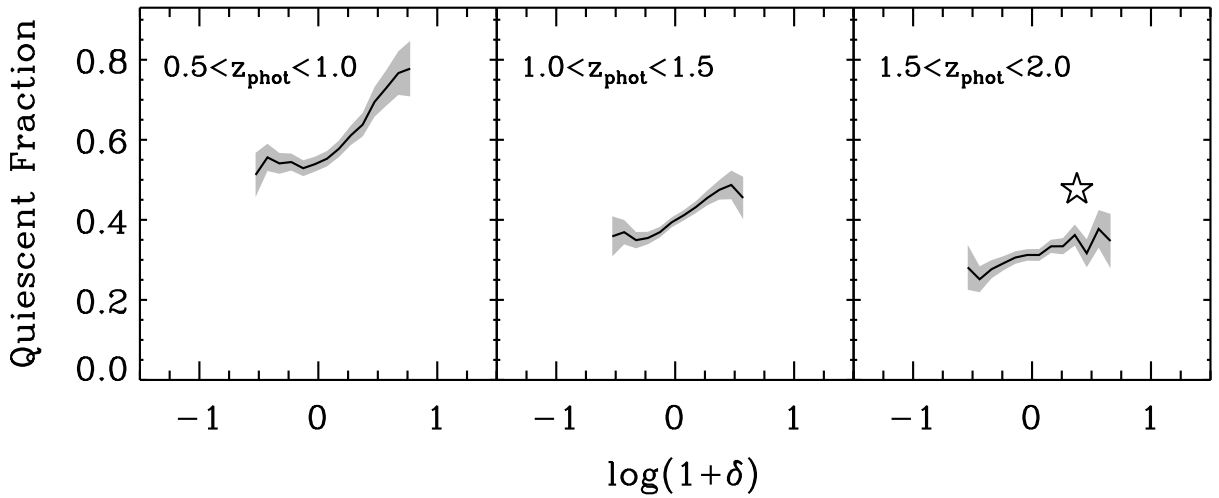


FIG. 2.— The quiescent fraction versus projected environmental density in three different redshift ranges for mass-selected samples. A limit of $\log(M/M_{\odot}) > 10.2$, which corresponds to our mass completeness limit at $z = 2$, is applied in all three panels. The quiescent fractions are determined using a running mean in a box that is 0.3 dex in $\log(1 + \delta)$, and the shaded region indicates the Poisson uncertainties. Even given the significant uncertainties introduced by photometric redshift errors, a clear SF-density relation is found at each redshift. The star in the rightmost panel shows the typical density and the quiescent fraction of galaxies in the $z = 1.6$ cluster described in §5. The cluster galaxies have a significantly higher quiescent fraction than the rest of the field.

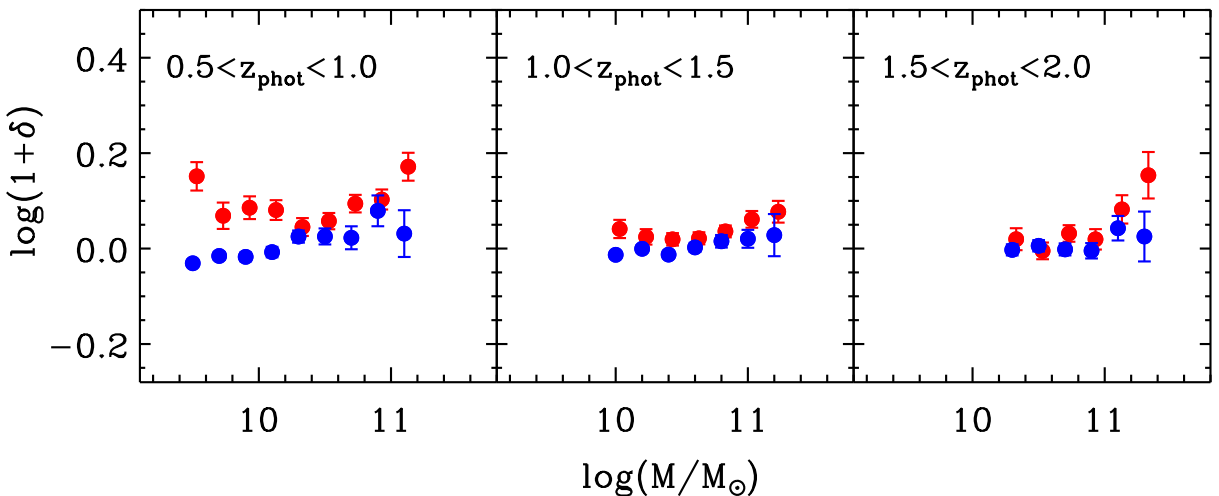


FIG. 3.— The average density versus stellar mass for star-forming galaxies (blue) and quiescent galaxies (red) in 0.2 dex mass bins. The red points have been offset slightly to higher masses for clarity. The quiescent galaxies tend to have higher densities than the star-forming galaxies even at fixed mass, implying that the SF-density relation is not simply the result of an underlying mass-density relation combined with a mass-SF relation. As explained in the text, the upturn in the densities for low-mass quiescent galaxies suggests that the environment plays a more important role in quenching star formation than for higher-mass galaxies. There is also a relationship between stellar mass and density at all redshifts, implying that the mass function varies with environment.

lar mass. However the relation is different for quiescent galaxies; low-mass quiescent galaxies are typically found in *denser* regions than quiescent galaxies of intermediate mass. This is a strong effect out to $z \sim 1$, and there is also a hint of it over $1 < z < 1.5$. A similar trend of increasing densities at the lowest masses has been found in the local universe using near-neighbor statistics by e.g. Hogg et al. (2003), and there is also evidence for it in the correlation functions of Norberg et al. (2002) and Zehavi et al. (2005). This result can be understood if the low-mass quiescent galaxies are primarily satellites in

groups or clusters. Such galaxies would be forming stars if they were in the field, but the star formation was shut off sometime after they were accreted into larger systems. Indeed, van den Bosch et al. (2008) use SDSS group catalogs to show that the majority of quiescent galaxies with $\log(M/M_{\odot}) < 10$ are satellites, and point to strangulation as the primary physical mechanism responsible for quenching the star formation. In the Appendix we use results from §4.3 to demonstrate more directly how the trends in the left panel of Figure 3 can be understood.

Another feature worth noting in Figure 3 is the simple

fact that there is a relationship between stellar mass and environmental density. This immediately implies that the mass function has some environmental dependence, which was already suggested by the clustering results of Wake et al. (2011).

Another way to test whether the observed SF-density relation is simply due to a stellar mass effect is by creating control samples of star forming galaxies to compare against the quiescent galaxies. For each quiescent galaxy, we find a matching object from among the star forming sample which has a similar mass and photometric redshift. We draw from the star forming galaxies without replacement. Since quiescent galaxies dominate the mass function at high masses, there are not enough star forming galaxies to make even a single complete control sample. If we cannot match a quiescent galaxy with a star forming galaxy, then it is removed. Conversely, star forming galaxies strongly dominate at lower masses, so low mass quiescent galaxies have many possible matches. In order to recover some of the information that we lose by not using all of the quiescent galaxies at the massive end, and not all of the star forming galaxies at the low-mass end, we repeat this procedure several times in order to create matched sets of quiescent and star forming galaxies. Although a more sophisticated comparison of the star forming and quiescent galaxies is certainly possible, this method is straightforward and adequate for our purposes.

Over the redshift ranges considered in Figures 2 and 3, none of the control samples of star-forming galaxies have mean density that is higher than the quiescent samples. A K-S test shows a $\ll 1\%$ chance that the distribution of densities for the quiescent galaxies and the matched star-forming galaxies are drawn from the same distribution in our lower redshift bins. This quantity increases to 2% at $1.25 < z_{phot} < 1.75$, suggesting that even at $z \sim 1.5$, environmental effects can be discerned at fixed stellar mass (see Figure 4). However at $1.5 < z_{phot} < 2$, this probability increases further to 24%, which means that if there is an environmental effect at fixed mass at over these redshifts then we are not able to detect it with significance.

4.3. The relationship between quenching efficiency and stellar mass

Given that the galaxies of all masses are subject to an SF-density relation out to at least $z \sim 1.5$, it is interesting to consider whether the environment affects different galaxies in different ways. In particular, it may be expected that the low-mass galaxies are affected more strongly than high-mass galaxies. This does not appear to be true at lower redshifts: van den Bosch et al. (2008) and Peng et al. (2010) show that the strength of environmental effects are independent of stellar mass at $z \sim 0$ (see also Baldry et al. 2006). Peng et al. (2010) also show this at $z \sim 0.5$ (see their Figure 7), and suggest that it remains true at even higher redshifts.

A first illustration of the effects of environment as a function of stellar mass is shown in Figure 5. If the strength of the environmental effects decreases strongly with increasing stellar mass, it is not apparent in this figure.

However, it is more useful to inspect what we term the *environmental quenching efficiency*, which is the fraction

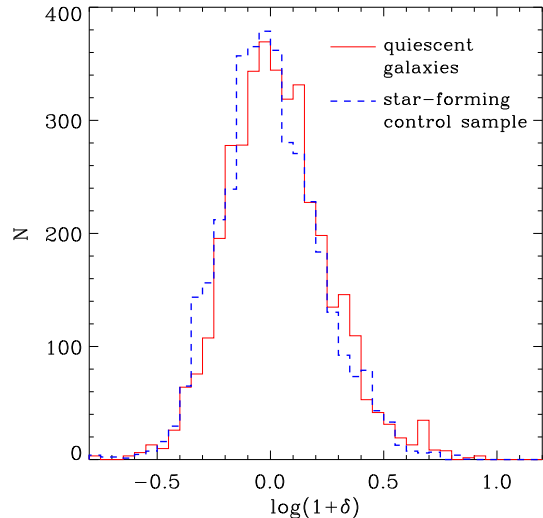


FIG. 4.— The distribution of densities for quiescent galaxies over $1.25 < z < 1.75$, and for a control sample of star-forming galaxies selected to have similar masses and redshifts. A K-S test indicates that the probability that these two distributions are drawn from the same parent distribution is 2%.

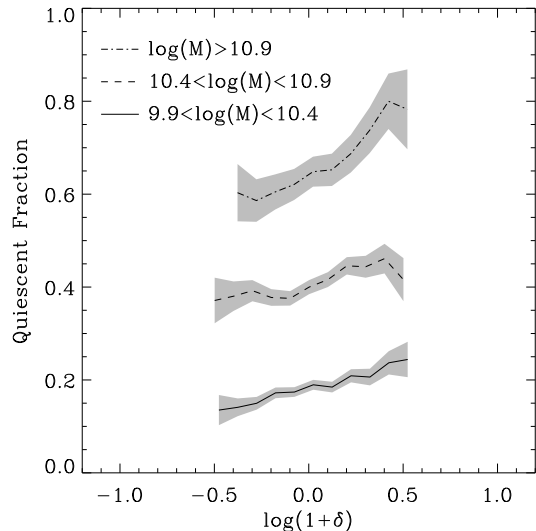


FIG. 5.— The quiescent fraction versus environmental density at $1 < z < 1.5$ for three different ranges in stellar mass. An SF-density relation is present in each of the mass bins.

of galaxies that would be star-forming if they were in low-density environments, but have had their star formation quenched due to some process related to the environment (van den Bosch et al. 2008; Peng et al. 2010). This is calculated as

$$\varepsilon_q = \frac{f_q(1+\delta) - f_q(1+\delta_0)}{f_{sf}(1+\delta_0)}, \quad (1)$$

where f_q is the quiescent fraction, $f_{sf} = 1 - f_q$ is the star-forming fraction, and $(1 + \delta_0)$ is some low-density “reference” environment. We use $\log(1 + \delta_0) = -0.4$; this choice is somewhat arbitrary, but for our purposes the exact value is not very important. Figure 6 shows

the quenching efficiency in different mass and redshift ranges. For clarity, we only show the uncertainties for the highest-mass bin in each panel. Although the uncertainties in this analysis are significant, it is apparent that the strength of environmental effect is largely independent of stellar mass out to at least $z \sim 1.25$, in agreement with the results from van den Bosch et al. (2008) and Peng et al. (2010) at lower redshifts.

Figure 6 also provides further illustration of the conclusion that the SF-density relation is not simply due to an underlying mass-density relation, since at the higher densities all galaxies—regardless of mass—have a positive quenching efficiency.

5. A CLUSTER AT $Z=1.6$

In the previous section we showed that the SF-density relation can be traced to at least $z \sim 1.5$ at fixed mass using a straightforward statistical comparison of the densities of star-forming and quiescent galaxies. Here, we provide a “case study” of a $z = 1.62$ galaxy cluster in the UDS field. This cluster was independently identified by Papovich et al. (2010) and by Tanaka et al. (2010), and has been detected in deep *XMM* imaging (even after removal of point sources; Tanaka et al. 2010), making it currently the second highest-redshift cluster with an x-ray detection. We follow Tran et al. (2010) in choosing the galaxy located at (2:18:21.09, -5:10:33.1) as the center of the cluster, as it is near the centroid of the galaxy overdensity, near the peak of the x-ray emission, and is the brightest cluster candidate in the NIR and *IRAC* bands.

We select cluster candidates as objects that lie within a projected distance of 1 comoving Mpc from the cluster center, which is roughly the radius containing the primary overdensity. Figure 7 shows the photometric redshift distribution of objects within this projected distance. There is a strong peak at the cluster redshift. As illustrated in the figure, we select as candidates objects at $1.3 < z_{phot} < 1.9$ ⁸.

As a large majority of the cluster candidates will actually lie in the cluster, we re-calculate the stellar masses and rest-frame colors of all candidates after fixing their redshift to $z = 1.62$, and apply the mass completeness limit of $10^{10} M_{\odot}$. Figure 8 shows a color-mass diagram, with quiescent galaxies marked in red and star-forming galaxies in blue. Quiescent galaxies dominate at $\log(M/M_{\odot}) > 11$ and star-forming galaxies dominate at $\log(M/M_{\odot}) < 10.5$ – but note that there are quiescent galaxies even at these relatively low masses. Figure 8 also shows those galaxies that are detected at $> 35 \mu\text{Jy}$ (corresponding to $\sim 3\sigma$) in the *MIPS* $24 \mu\text{m}$ band. With a single exception, the more massive star-forming galaxies are detected while the quiescent galaxies and the less massive star-forming galaxies are not. Finally, we point out that there is no clear bimodality visible in this figure; this is mostly because several of the star-forming galaxies are highly reddened, so they contaminate the

red sequence (see also Tran et al. 2010).

The masses for the cluster candidates are shown with the black histogram in Figure 9. There will be some contamination by field galaxies in our cluster sample, but this should not be a significant issue considering that this region is overdense by a factor of 5. We illustrate the expected contamination with the dashed blue histogram in Figure 9. The expected mass distribution of the contaminants was calculated in the same way as for the cluster candidates: we select all field objects with $1.3 < z_{phot} < 1.9$, force their redshifts to $z = 1.6$, and re-calculate the masses.

In Figure 9 we also compare the number of quiescent cluster candidates (red hatched histogram) with the number that would be expected in the absence of an SF-density relation (purple hatched histogram). This latter quantity is calculated by multiplying the mass distribution of all cluster candidates by the mass-dependent quiescent fraction that is determined from the field. A comparison of the hatched histograms shows that the number of quiescent objects (10) is larger than the expected number of quiescent objects (5.6). This immediately suggests the presence of an SF-density relation even at fixed mass.

This conclusion is made more explicit in Figure 10, which shows the quenching efficiency for this cluster in two broad (0.7 dex) mass bins. The quenching efficiency is calculated in analogy with equation 1, where the low-density “reference” environment is taken to be the field and the higher-density environment is the cluster.⁹ In this figure we have also performed (small) corrections for the estimated contamination. The uncertainties in the quiescent fraction are calculated using the Wilson interval for binomial statistics, which is appropriate for the small numbers considered here.

Although the uncertainties are large due to the limited sample size, there does appear to be a boosted quenching efficiency in each of our (independent) mass bins. Also, as was already shown in Figure 6 at somewhat lower redshifts, there is no suggestion that the quenching efficiency depends on stellar mass. The grey shaded region in this figure illustrates the range of quenching efficiencies determined by van den Bosch et al. (2008) for satellite galaxies in groups in the SDSS. Although the large uncertainties obviously prevent us from drawing strong conclusions, it is striking that the quenching efficiency at $z = 1.6$ is consistent with that at $z \sim 0$.

We note that Tran et al. (2010) have also investigated the star formation in this cluster. Those authors note that a significant number of the cluster candidates are detected at $24 \mu\text{m}$, and are therefore likely to be strongly star-forming. They also emphasize that this situation is different than for clusters at $z \lesssim 1$, where a larger fraction of galaxies are dead. Here we emphasize a complementary point: while it is true that a significant fraction of the cluster members are forming stars at a high rate, nonetheless the fraction of quiescent objects is *still* higher than in the field at similar redshifts.¹⁰ Thus, a

⁸ This redshift range corresponds to a photometric redshift error of $\pm 2\sigma$ at the cluster redshift, which means that in principle some cluster members may escape our criteria. However we have tried increasing the search range to 3σ , and a close inspection of SEDs of the additional objects suggests that none of them are actual cluster members. Thus using a broader redshift range would only increase the contamination from field galaxies.

⁹ Since many of these “field” galaxies will also be in groups, and will therefore have experienced some quenching due to environmental processes, our quenching efficiencies will be biased slightly low.

¹⁰ There are a number of differences between our analysis and that of Tran et al. (2010). The most important appears to be that they identify cluster candidates within 1 physical Mpc, whereas

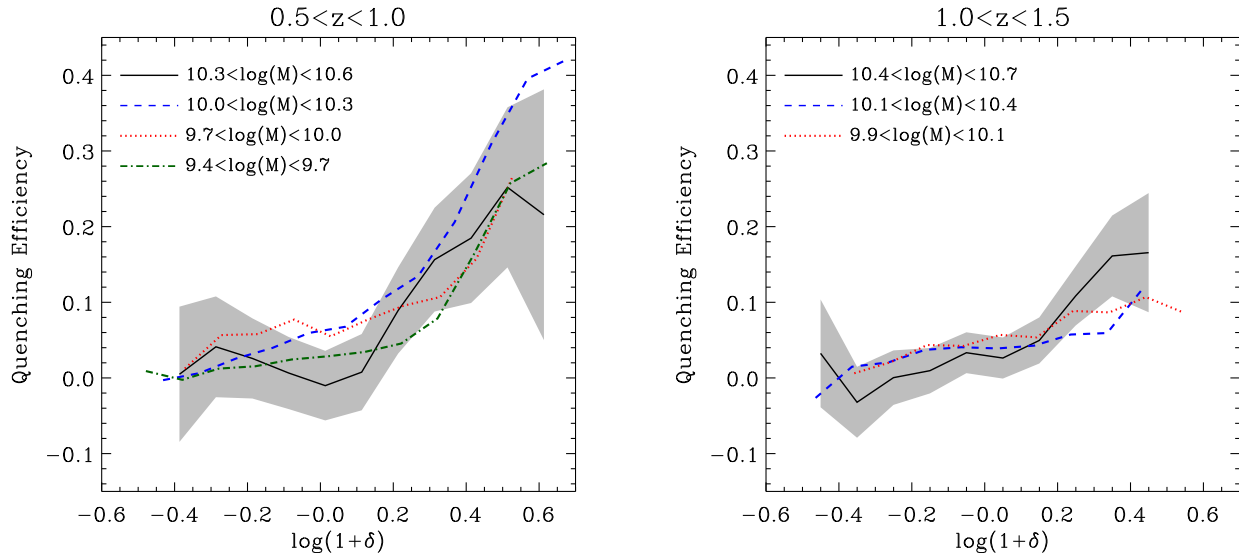


FIG. 6.— The quenching efficiency versus local density. The quenching efficiency is defined as the fraction of galaxies that would be forming stars if they were found in a low-density environment, but have had their star formation quenched. The shaded region shows the uncertainties for only the high-mass bins. The quenching efficiency appears to be largely independent of stellar mass.

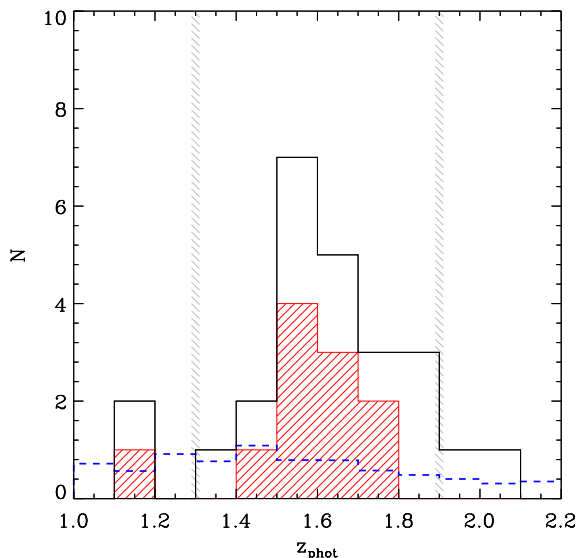


FIG. 7.— Photometric redshift distribution of objects in the vicinity of the cluster at $z = 1.62$. The solid black histogram is for all objects that have a stellar mass $M > 10^{10} M_{\odot}$ at the best-fitting photometric redshift, and the red hatched histogram shows which of those objects are classified as quiescent. The blue dashed histogram shows the expected contamination from field galaxies. The grey vertical hatched regions show the photometric redshift range that we use to identify candidate cluster members.

we use 1 comoving Mpc; their larger radius will include significantly more contamination from field galaxies, and will include more galaxies on the lower-density outskirts of the cluster which may be expected to have increased SF activity. A second difference is that we use mass-selected samples. The fact that Tran et al. (2010) focus on star formation rates derived from $24\mu\text{m}$ imaging, whereas we classify galaxies according to the color bimodality, is less material: we find that $\sim 20\%$ of the cluster candidates are detected at $> 35\mu\text{Jy}$ at $24\mu\text{m}$, whereas this increases to $\sim 40\%$ over the rest of the field. Despite the differences in methods, Tran et al. (2010) do find a quiescent fraction that is similar to ours (see the bottom panel of their Figure 3).

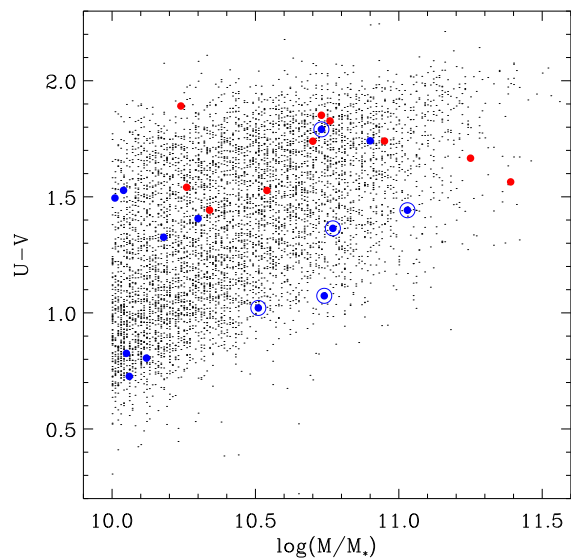


FIG. 8.— Rest-frame color versus stellar mass for the candidate cluster galaxies. Objects that are classified as quiescent according to §2.3 are shown with red symbols, while star-forming galaxies are in blue. Objects that are detected at $24\mu\text{m}$ are circled. Quiescent galaxies in this cluster are found over the entire mass range, and dominate at the highest masses. At high masses there is good correspondence between a $24\mu\text{m}$ detection and our classification of galaxies as star-forming, while quiescent galaxies and lower-mass star-forming galaxies are not detected. The small black points represent field galaxies.

SF-density relation appears to be in place at $z = 1.6$ with no evidence of a reversal.

6. SUMMARY AND DISCUSSION

In this paper we have studied the evolution of the star formation-density relation, in which quiescent galaxies are found preferentially in dense environments. We have used public data from the UKIDSS-UDS and have constructed mass-limited samples, rather than flux- or luminosity-limited samples, in order to obtain a better

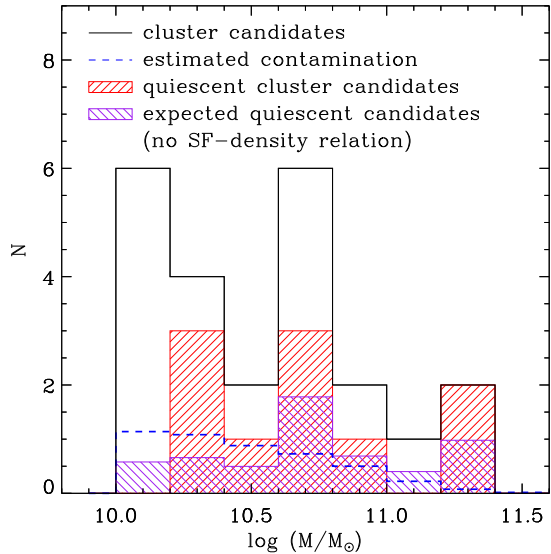


FIG. 9.— Histograms of stellar masses for candidate members for a cluster at $z = 1.62$. The black and red-hatched histograms are for the candidates and the subset of quiescent candidates. The blue dashed histogram shows the estimated contamination from field galaxies; a comparison with the black histogram shows that contamination is minimal. The purple hatched histogram shows the black histogram multiplied by the quiescent fraction as a function of mass that is determined from field galaxies; this illustrates the expected number of quiescent cluster candidates in the absence of an SF-density relation, and a comparison between the red- and purple-hatched histograms shows that an SF-density relation is in place.

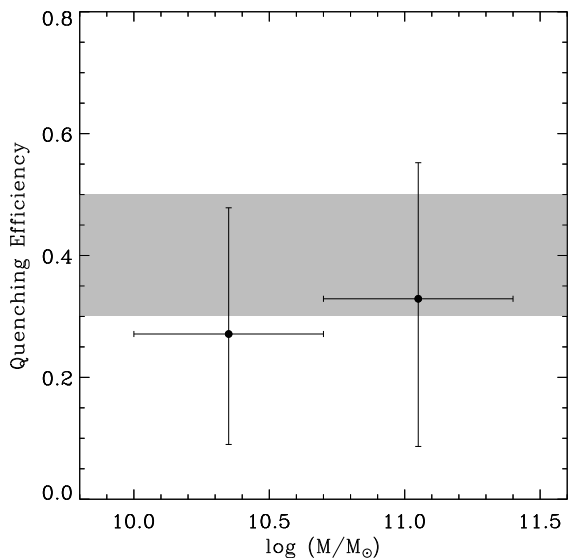


FIG. 10.— The quenching efficiency in two broad stellar mass bins for the candidate cluster members. The quenching efficiency is defined as the fraction of galaxies that would be forming stars if found in the field, but have had their star formation quenched. Although the uncertainties are large, there is a positive quenching efficiency in both mass bins (i.e. there is a SF-density relation in this cluster), and there is no evidence that the quenching efficiency depends on stellar mass. The grey shaded region shows the range of quenching efficiencies for satellite galaxies in SDSS groups from van den Bosch et al. (2008). Within the uncertainties, the quenching efficiency at $z \sim 1.6$ is consistent with that at $z \sim 0$.

understanding of environmental effects and to avoid the selection effects that have been prevalent in several previous studies. Quiescent galaxies are identified according to the observed bimodality in a rest-frame color-color diagram; we prefer this method over the use of a standard color-magnitude diagram as it cleanly separates galaxies that are red due to dust from galaxies that are red due to a lack of significant star formation. Environmental densities are measured by counting near neighbors. Because large and representative samples of spectroscopic redshifts are not currently available at $z > 1$, in this work we rely on photometric redshifts. This introduces large uncertainties in the density measurements and, as discussed in §2, can also potentially introduce spurious environmental trends if the effects of redshift errors are not correctly taken into account.

Even with the uncertainties inherent in our analysis, we find that the SF-density relation can be traced to at least $z \sim 1.8$, which is higher than previous studies have found using either photometric or spectroscopic redshifts (but see Chuter et al. 2011, who have recently used earlier data in the UDS to arrive at a similar conclusion). We show that, out to at least $z \sim 1.5$, the SF-density relation is not simply the result of a mass-density relation combined with a mass-SF relation: even at fixed mass galaxies in denser environments have a higher quiescent fraction.

Nevertheless we do find a relationship between stellar mass and environment. As shown in Figure 3, this relationship is straightforward for star-forming galaxies in that more massive galaxies tend to be found in denser environments. The situation is more complicated for quiescent galaxies: both low-mass ($\log(M/M_\odot) \lesssim 10.3$) and high-mass quiescent galaxies tend to be found in the densest environments, whereas at intermediate masses galaxies are also found at lower densities. This is a known feature of the low-redshift universe (Hogg et al. 2003; van den Bosch et al. 2008; see also Ross et al. 2010), and we have found that it remains in place out to at least $z \sim 1$. As we demonstrate in the Appendix, this relationship can be understood if low-mass quiescent galaxies occur primarily at high densities because environmental processes are required to shut off the star formation. At intermediate masses there are other processes (e.g. AGN feedback) that can also play a role; such galaxies may thus also be found in comparatively low-density environments. At even higher masses galaxies tend to be found in groups and clusters regardless of whether they are forming stars. This reasoning implies that the environment plays a greater role in the build-up of the red sequence at lower masses (Fig. 13; see also van den Bosch et al. 2008). It also implies that the shape of the mass function has significant environmental dependence at $z \sim 1$. For the star-forming galaxies, we expect that dense environments should have a greater number of massive galaxies when compared to the field. For the passive galaxies, we expect that dense environments have a greater number of high-mass *and* low-mass galaxies.

We find that environmental quenching operates on all galaxies, with no evidence that the quenching efficiency depends on stellar mass. Similar results have been obtained at lower redshifts by van den Bosch et al. (2008) and Peng et al. (2010).

Most of our conclusions receive additional support from our analysis of the central regions of a cluster at $z = 1.62$. The photometrically-selected candidate cluster members tend to have higher stellar masses than field galaxies, and have a higher quiescent fraction even at fixed mass. Although the uncertainties are very large, there does not appear any variation in the quenching efficiency with mass within the cluster. Interestingly, the quenching efficiency is also consistent with that found by van den Bosch et al. (2008) for low-redshift galaxy groups and clusters in SDSS. This is also in agreement with the suggestion by Peng et al. (2010), who find that the environmental quenching efficiency does not evolve significantly at $z < 1$. But, as pointed out by those authors, environmental processes may still play a greater role at lower redshifts as more galaxies will have been accreted into dense environments. In this paper we have only considered galaxies in the central regions of a single cluster; it would clearly be beneficial to extend this analysis to a greater number of high-redshift clusters, and to look for variations in galaxy properties with cluster-centric distance (e.g. Patel et al. 2009a).

The results presented here have implications for our understanding of the physical processes that work to quench star formation in dense environments. It is thought that strangulation — the stripping of halo gas from galaxies as they are accreted into larger systems — is largely responsible, but that this is a gradual process that acts over the course of a couple Gyr (e.g. McCarthy et al. 2008; McGee et al. 2009; Weinmann et al. 2010). If this remains the case at high redshift then it is expected that environmental effects should cease to be observable since satellite systems can only have been accreted recently. Indeed, McGee et al. (2009) predict that environmental trends should be weak or non-existent at $z \sim 1.5$. Even with the large uncertainties introduced by our use of photometric redshifts, we do find an SF-density relation in place at this redshift. It may be that the relevant timescales (for gas stripping, and for the consumption of gas that hasn't been stripped) are shorter at these redshifts (Weinmann et al. 2010; Tinker & Wetzel 2010). Other physical processes that operate in dense environments may also play a role. Another slightly more exotic possibility is that, one way or another, the galaxies “knew” beforehand that they would be accreted and had already shut off their star formation; such an effect would presumably be related to the “assembly bias” of dark matter halos (see discussion by Quadri et al. 2008; Tinker et al. 2010; Neistein et al. 2010). Unfortunately we cannot detect nor completely rule out a relation at significantly higher redshifts to provide tighter constraints.

Our result that the environmental quenching efficiency does not show a strong dependence on stellar mass — which echoes recent results at lower redshifts — may present an interesting challenge, as strangulation is expected to be somewhat more effective for low-mass galaxies (e.g. McCarthy et al. 2008). Although the uncertain-

ties are large, our analysis of the $z = 1.6$ cluster suggests that the environmental quenching efficiency is not greatly reduced compared to at $z \sim 0$. This may also present interesting constraints, as galaxies in this cluster can only have been accreted recently so environmental processes have had a much longer time to operate at $z \sim 0$ than at $z \sim 1.6$.

In this paper we have investigated the fraction of quiescent objects as a function of local density. We note that, at least in principle, it is possible that other measures of environmental influence — such as the average star formation rate per galaxy or the fraction of galaxies undergoing intense starbursts — would yield different results. Similarly, the color-density relation may evolve differently since many “red” galaxies have obscured star formation, and the morphology-density relation may also evolve differently (Capak et al. 2007). Future work would do well to investigate each of these relationships.

The analysis that has been presented in this paper is quite basic, and can be extended and improved upon in several ways. It may not be completely straightforward to significantly improve on the simplest density estimators similar to the one used in this paper using standard broadband photometric redshifts, and obtaining very large and unbiased samples of spectroscopic redshifts beyond $z \sim 1$ remains difficult. More sophisticated means of constructing the density field that include both photometric and spectroscopic redshifts provide one direction forward (Kovač et al. 2010). Another difficulty lies in a detailed physical interpretation of environmental densities. In the Λ CDM context, it is not necessarily the number of near neighbors that is the most relevant physical quantity; more relevant “observables” include halo mass, whether a galaxy is a central or satellite, and perhaps group- or cluster- centric distance. Nearest-neighbor statistics mix all of these quantities. Thus it may be more promising to identify groups, and to distinguish between centrals and satellites in the same way that has been done at lower redshifts. However this procedure is also problematic, as identifying group members is not trivial and, as groups should be rapidly assembling at these redshifts, the central/satellite distinction may be less meaningful.

This work is based on data obtained as part of the UKIRT Infrared Deep Sky Survey. We thank Gabe Brammer for help with the photometric redshifts, as well as Simone Weinmann, Shannon Patel, and Olivera Rakic for their careful reading of a draft version of this manuscript. Support for this work was provided by NASA through Hubble Fellowship grant #51279.01 awarded by the Space Telescope Science Institute, which is operated by the Association of Universities for Research in Astronomy, Inc., for NASA, under contract NAS 5-26555.

REFERENCES

- Baldry, I. K., Balogh, M. L., Bower, R. G., Glazebrook, K., Nichol, R. C., Bamford, S. P., & Budavari, T. 2006, *MNRAS*, 373, 469
- Balogh, M. L., Schade, D., Morris, S. L., Yee, H. K. C., Carlberg, R. G., & Ellingson, E. 1998, *ApJ*, 504, L75
- Brammer, G. B., van Dokkum, P. G., & Coppi, P. 2008, *ApJ*, 686, 1503

- Brammer, G. B., et al. 2009, ApJ, 807, L173
 Bruzual, G., & Charlot, S. 2003, MNRAS, 344, 1000
 Capak, P., Abraham, R. G., Ellis, R. S., Mobasher, B., Scoville, N., Sheth, K., & Koekemoer, A. 2007, ApJS, 172, 284
 Chuter, R. W., et al. 2011, MNRAS, in press (arXiv:1101.0849)
 Cooper, M., et al. 2007, MNRAS, 376, 1445
 Cooper, M., et al. 2010, MNRAS, 409, 337
 Cucchiati, O., et al. 2006, A&A, 458, 39
 Dressler, A. 1980, ApJ, 236, 351
 Elbaz, D., et al. 2007, A&A, 468, 33
 Furusawa, H., et al. 2008, ApJS, 176, 1
 Gómez, P. L. et al. 2003, ApJ, 584, 210
 Grazian, A., et al. 2006, A&A, 453, 507
 Grützbauch, R., Chuter, R. W., Conselice, C. J., Bauer, A. E., Bluck, A. F. L., Buitrago, F., Mortlock, A. 2010, MNRAS, accepted (arXiv:1011.4846)
 Grützbauch, R., Conselice, C. J., Varela, J., Bundy, K., Cooper, M. C., Skibba, R., & Willmer, C. N. A. 2011, MNRAS, 411, 929
 Hartley, W. G., et al. 2010, MNRAS, 407, 1212
 Hewett, P. C., Warren, S. J., Leggett, S. K., & Hodgkin S. T. 2006, MNRAS, 367, 454
 Hodgkin, S. T., Irwin, M. J., Hewett, P. C., & Warren, S. J. 2009, MNRAS, 394, 675
 Hogg, D. W., et al. 2003, ApJ, 585, L5
 Ideue, Y., et al. 2009, ApJ, 700, 971
 Ilbert, O., et al. 2010, ApJ, 709, 644
 Iovnio, A., et al. 2010, A&A, 509, 40.
 Kajisawa, M., Ichikawa, T., Yoshikawa, T., Yamada, T., Onodera, M., Akiyama, M., & Tanaka, I. 2011, PASJ, accepted (arXiv:1101.0001)
 Kauffmann, G., White, S. D. M., Heckman, T. M., Ménard, B., Brinchmann, J., Charlot, S., Tremonti, C., & Brinkmann, J. 2004, MNRAS, 353, 731
 Kovač, K., et al. 2010, ApJ, 708, 505
 Kriek, M., van Dokkum, P. G., Labbé, I., Franx, M., Illingworth, G. D., Marchesini, D., & Quadri, R. F. 2009, ApJ, 700, 221
 Kurk, J., et al. 2009, A&A, 504, 331
 Labbé, I., Bouwens, R., Illingworth, G. D., & Franx, M. 2006, ApJ, 649, L67
 Lawrence, A., et al. 2007, MNRAS, 379, 1599
 Lonsdale, C. J., et al. 2003, PASP, 115, 897
 Maraston, C. 2005, MNRAS, 362, 799
 Marchesini, D. et al. 2009, ApJ, 701, 1765
 McCarthy, P. J., et al. 2007, ApJ, 664, L17
 McCarthy, I. G., Frenk, C. S., Font, A. S., Lacey, C. G., Bower, R. G., Mitchell, N. L., Balogh, M. L., & Theuns, T. 2008, MNRAS, 383, 593
 McGee, S. L., Balogh, M. L., Bower, R. G., Font, A. S., & McCarthy, I. G. 2009, MNRAS, 400, 937
 Neistein, E., Weinmann, S. M., Li, C., & Boylan-Kolchin, M. 2010, MNRAS, in press (arXiv:1011.2492)
 Norberg, P., et al. 2002, MNRAS, 332, 827
 Papovich, C., et al. 2010, ApJ, 716, 1503
 Patel, S. G., Kelson, D. D., Holden, B. P., Illingworth, G. D., Franx, M., van der Wel, A., & Ford, H. 2009, ApJ, 694, 1349.
 Patel, S. G., Holden, B. P., Kelson, D. D., Illingworth, G. D., & Franx, M. 2009, ApJ, 705, L67
 Patel, S. G., Kelson, D. D., Holden, B. P., Franx, M., & Illingworth, G. D. 2011, ApJ, submitted (arXiv:1104.0934)
 Peng, Y., et al. 2010, ApJ, 721, 193
 Quadri, R., et al. 2007, ApJ, 654, 138
 Quadri, R. F., et al. 2008, ApJ, 685, L1
 Quadri, R. F., & Williams, R. J. 2010, ApJ, 725, 794
 Ross, A. J., Tojeiro, R., & Percival, W. J. 2010, MNRAS, in press (arXiv:1010.1403)
 Salimbeni, S., et al. 2009, A&A, 501, 865
 Scoddeggio, M., et al. 2009, A&A, 501, 21
 Scoville, N., et al. 2007, ApJS, 172, 150
 Smail, I., Sharp, R., Swinbank, A. M., Akiyama, M., Ueda, Y., Foucaud, S., Almaini, O., & Croom, S. 2008, MNRAS, 389, 407
 Strazzullo, V., et al. 2010, A&A, 524, A17
 Tanaka, M., Finoguenov, A., & Ueda, Y. 2010, ApJ, 716, L152
 Tinker, J. L., Wechsler, R. H., & Zheng, Z. 2010, ApJ, 709, 67
 Tinker, J. L., & Wetzel, A. R. 2010, ApJ, 719, 88
 Tran, K. H., et al. 2010, ApJ, 719, L126
 van den Bosch, F. C., Aquino, D., Yang, X., Mo, H. J., Pasquali, A., McIntosh, D. H., Weinmann, S. M., & Kang, X. 2008, MNRAS, 387, 79
 Weinmann, S. M., van den Bosch, F. C., Yang, X., & Mo, H. J. 2006, MNRAS, 366, 2
 Weinmann, S. M., Kauffmann, G., von der Linden, A., & De Lucia, G. 2010, MNRAS, 406, 2249
 Wake, D. A., et al. 2011, ApJ, 728, 46
 Whitaker, K., et al. 2010, ApJ, 719, 1715
 Williams, R. J., Quadri, R. F., Franx, M., van Dokkum, P., & Labbé, I. 2009, ApJ, 691, 1879
 Wilson, G., et al. 2009, 698, 1943
 Zehavi, I. et al. 2005, ApJ, 630, 1

APPENDIX

THE DIFFERENT MASS-DENSITY RELATIONS FOR STAR-FORMING AND QUIESCENT GALAXIES, AND IMPLICATIONS FOR THE BUILD-UP OF THE RED SEQUENCE

The leftmost panel in Figure 3 shows a roughly monotonic increasing relationship between mean density and stellar mass for star-forming galaxies. But for quiescent galaxies the relationship is less trivial, since both low-mass and high-mass quiescent galaxies lie in denser regions than those of intermediate mass. This may seem counterintuitive, since low-mass galaxies are not expected to be particularly associated with high-density regions. In this appendix we use a simple model to show how these relationships might be understood, and to support our conclusion that — even though the efficiency of environmental quenching appears to be independent of stellar mass — the environment plays a larger role in building up the red sequence at lower masses than at higher masses. The treatment here is only meant to be illustrative and approximate, as a complete treatment would require better three-dimensional density estimates over a wide dynamic range than is possible using our simple and purely photometric projected density measurements.

Our approach is similar to that taken previously by Peng et al. (2010), and involves three basic ingredients. The first is a mass-density relation, in which more massive galaxies tend to lie in denser regions. The second is the environmental quenching, which we calculate as described in §4.3. However there must be (at least) one other quenching mechanism. We will refer to this third ingredient as *mass quenching* as it is found to be a strong function of stellar mass. Roughly speaking, this results in the well-observed phenomenon that more massive galaxies are more likely to be quenched. We calculate the mass quenching from the fraction of quenched objects which are not explained by environmental quenching over the redshift range $0.5 < z_{phot} < 1$. The environmental and mass quenching efficiencies are shown in the two panels of Figure 11, and in both cases we fit a function of the form

$$\epsilon(\rho) = 1 - \exp(-\rho/p_1)^{p_2}. \quad (\text{A1})$$

We perform Monte Carlo simulations in which we take the observed masses and densities for galaxies at $0.5 <$

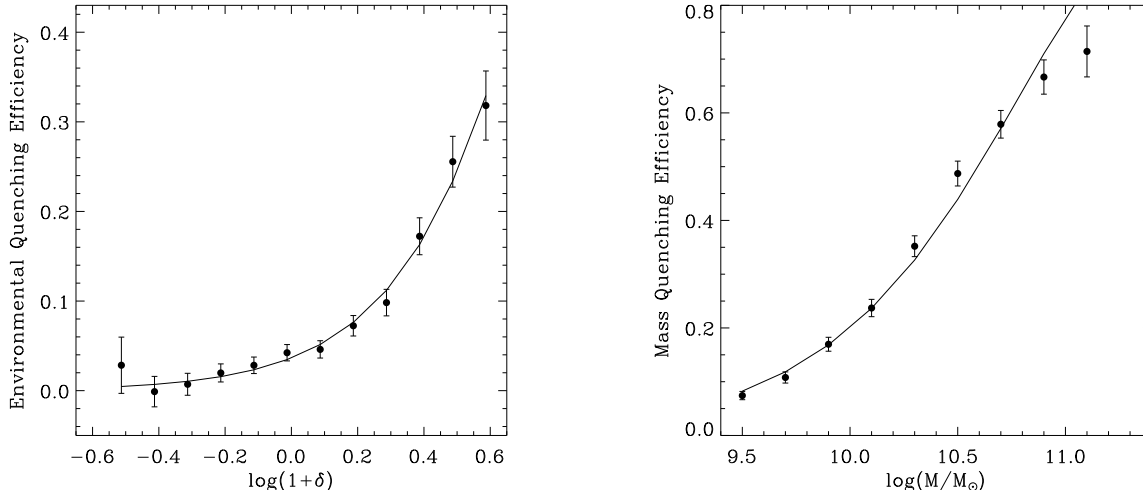


FIG. 11.— *Left*: The environmental quenching efficiency, which is defined as the fraction of galaxies that would be forming stars if they were found in low-density environments, but have had their star formation shut off by environmental processes. *Right*: The mass quenching efficiency, which is the residual quenching that is not explained by environmental quenching. This quenching process is a strong function of stellar mass. The solid curves in the two panels are fits to the data.

$z_{phot} < 1$ and randomly quench them according to the environmental and mass quenching efficiencies. The main result of these simulations is shown in the top left panel of Figure 12.

It is perhaps not surprising that the simulations more or less reproduce the measurements shown in Figure 3, as the simulations make use of the densities, mass quenching efficiency, and environmental quenching efficiency that we infer from the data. The key point is that the three ingredients described above are required to produce the characteristic shapes of the mass-density relations for both the star-forming and quiescent populations. In the remaining panels of Figure 12 we remove each of the three ingredients in turn in order to provide some insight into how they interact to produce these characteristic shapes. In the top right panel, we remove the environmental quenching; this has the obvious effect of eliminating the difference in densities between quenched and star-forming galaxies. In the bottom left panel we remove the mass quenching. In this case it is primarily the galaxies in the densest regions that are quenched, since mass quenching is not available to quench galaxies at less extreme densities. Finally, in the bottom right panel we remove the mass-density relation by randomizing the relationship between stellar mass and densities in our catalogs. In this case there is no relationship between mass and density for the star-forming galaxies, and there is no upturn at high masses for the quiescent galaxies. But there is a prominent upturn in the densities for low-mass quiescent objects. This is because mass quenching is very inefficient for those objects (Fig. 11) and so it is primarily the few low mass galaxies that are in very dense regions that are quenched. A consideration of the top right and bottom panels of Figure 12 shows how each of the three ingredients of the model interact to produce the shapes that are shown in the top left panel: the environmental quenching introduces a large offset between the star-forming and quiescent tracks, the mass quenching reduces the offset (doing so more effectively at intermediate and high masses than at low masses), and the mass-density relation causes the rise in densities at high masses for both the star-forming and quiescent galaxies.

In §4.2 and §6 it was argued that the U-shaped curve followed by the quiescent galaxies in the the plot of mass versus density suggests that the environment plays a more important role in building up the red sequence at lower masses. This is shown explicitly in Figure 13, which compares the mass and environmental quenching efficiencies as a function of stellar mass. The environmental quenching efficiency in this figure is calculated as the mean value for galaxies in bins of stellar mass. It is apparent that the mass quenching dominates significantly over the environmental quenching at all but the lowest stellar masses. It is only at these relatively low masses that environmental processes play a large role in building up the red sequence (see also van den Bosch et al. 2008). The fact that the environmental quenching efficiency is lower than the mass quenching efficiency does not mean that environment does not exert a strong influence; it merely reflects the fact that most galaxies are not in dense enough regions for environmental processes to have a large effect. In this appendix we have focused on the redshift range $0.5 < z < 1$, and it is expected that the curves shown in Figure 13 will evolve somewhat at lower and higher redshifts.

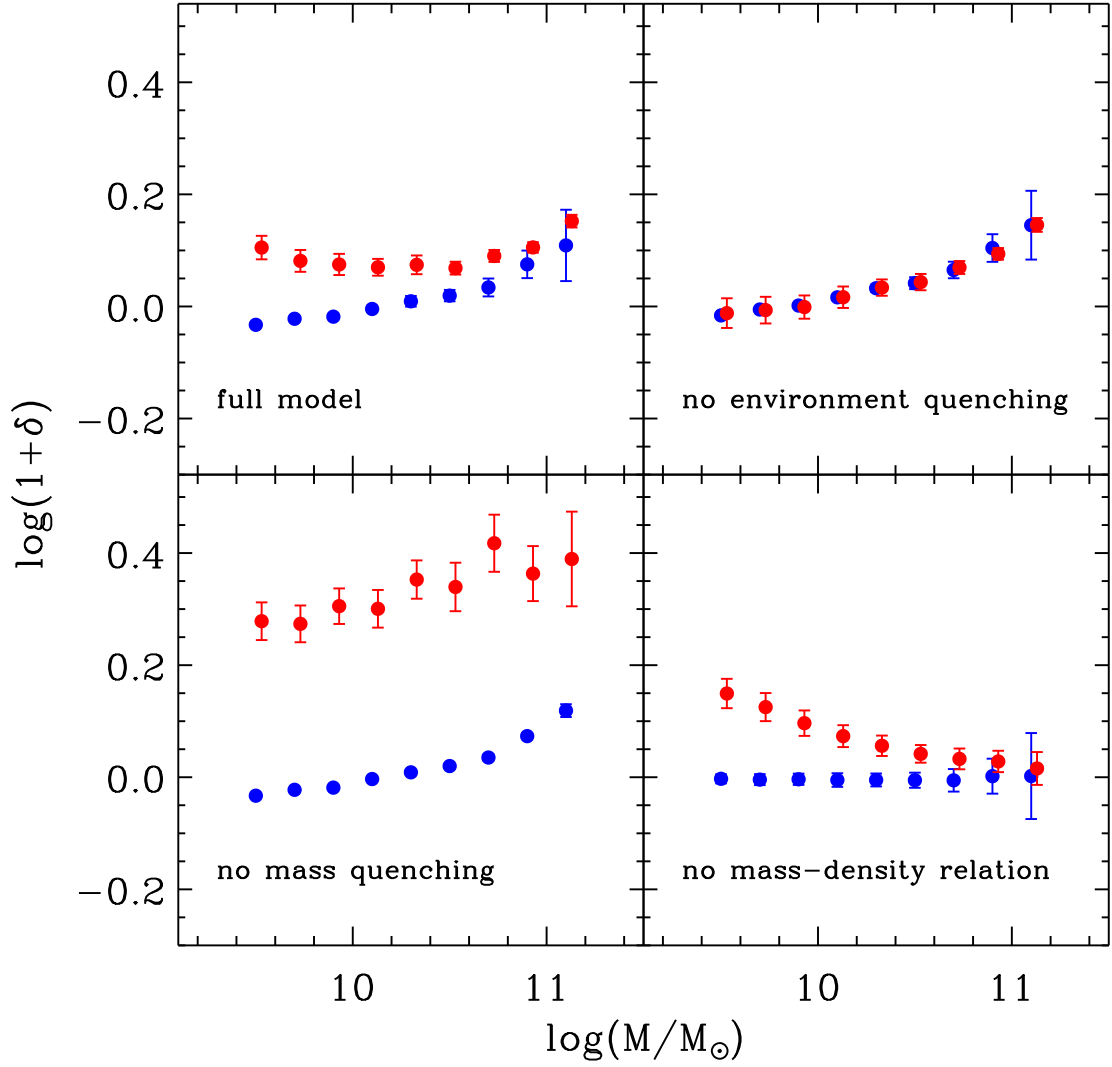


FIG. 12.— The top left panel shows the relationship between stellar mass and mean density for quiescent and star-forming galaxies (red and blue symbols, respectively) in our Monte Carlo simulations. The errorbars represent the scatter between the simulations, and the red symbols have been offset slightly to the right for clarity. This panel can be compared to the measurements shown in the leftmost panel of Figure 3. In the remaining three panels of this figure, we remove in turn each of the three ingredients in the Monte Carlo simulations. It is apparent that all three ingredients interact to produce the characteristic shapes in the top left panel.

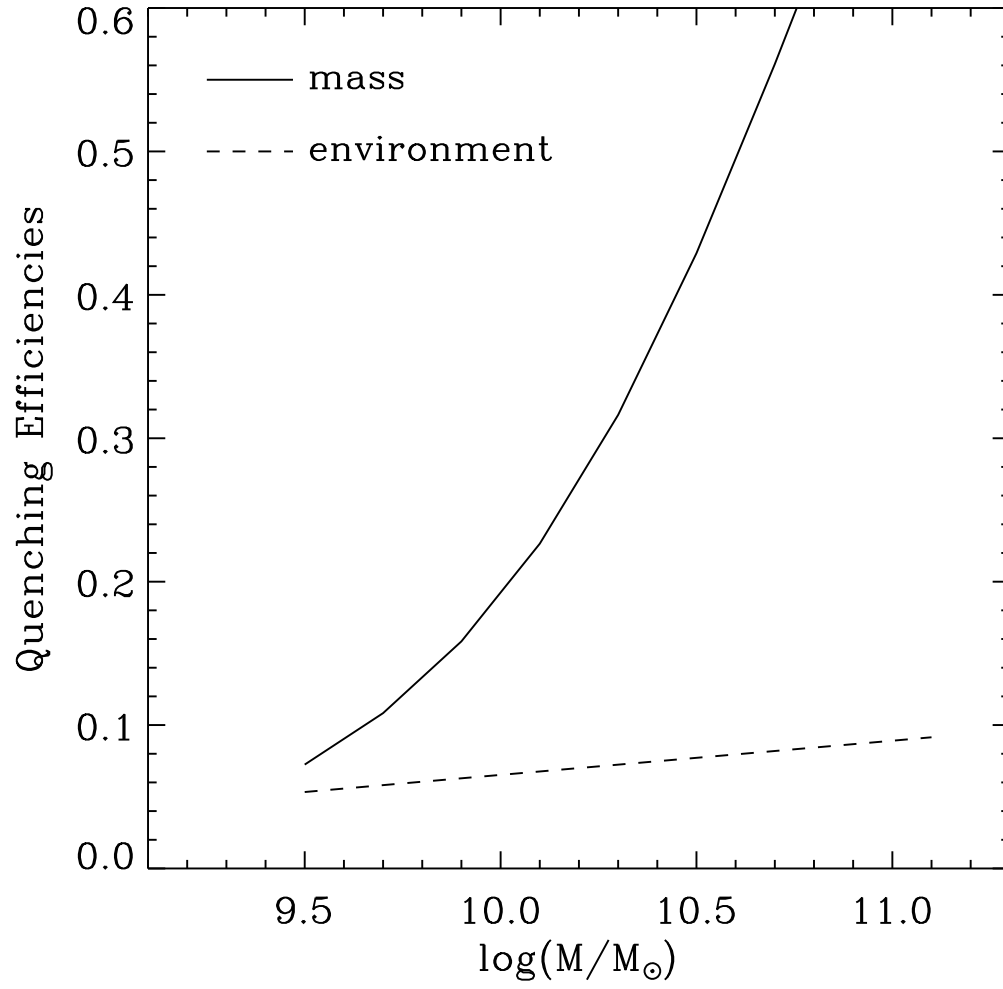


FIG. 13.— The mass and mean environmental quenching efficiencies as a function of stellar mass. Mass quenching dominates strongly over environmental quenching at all but the lowest stellar masses. This implies that environmental processes play a relatively small role in the buildup of the red sequence at high masses, but become increasingly important at lower masses.